Geophysical Research Letters

RESEARCH LETTER
10.1029/2019GL086539

Gravity Wave Influences On Mesoscale Divergence: An Observational Case Study

C. C. Stephan[1], T. P. Lane[2,3], and C. Jakob[3,4]

[1]Max Planck Institute for Meteorology, Hamburg, Germany, [2]School of Earth Sciences, The University of Melbourne, Melbourne, Victoria, Australia, [3]ARC Centre of Excellence for Climate Extremes, Sydney, New South Wales, Australia, [4]School of Earth, Atmosphere and Environment, Monash University, Melbourne, Victoria, Australia

Key Points:
- Mesoscale divergence profiles near Darwin show similar long-lived fine-scale vertical structure to that reported over the tropical Atlantic
- High-resolution soundings are used to test if gravity waves can serve as a plausible explanation for the observed divergence variability
- Results imply that spatial and temporal variability of mesoscale horizontal divergence are consistent with a forcing by gravity waves

Correspondence to:
C. C. Stephan,
claudia.stephan@mpimet.mpg.de

Citation:
Stephan, C. C., Lane, T. P., & Jakob, C. (2020). Gravity wave influences on mesoscale divergence: An observational case study. *Geophysical Research Letters*, *47*, e2019GL086539. https://doi.org/10.1029/2019GL086539

Received 6 DEC 2019
Accepted 30 DEC 2019
Accepted article online 3 JAN 2020

Abstract Characteristics of tropospheric low-frequency gravity waves are diagnosed in radiosonde soundings from the Tropical Warm Pool-International Cloud Experiment near Darwin, Australia. The waves have typical vertical wavelengths of about 4 km, horizontal wavelengths of about 600 km, and intrinsic periods of about 12 hr. These scales match those of the vertical, horizontal, and temporal variability found in area-averaged horizontal wind divergence over the same domain. Vertical profiles of divergence show wave-like structures with variability of the order of 2×10^{-5} s^{-1} in the free troposphere. The results for Darwin are similar to previously reported observed mesoscale patterns of divergence/convergence over the tropical Atlantic. The findings imply that tropical divergence on spatial scales of a few hundred kilometers, which is known to influence the organization of convection, may be forced by gravity waves.

Plain Language Summary On horizontal scales of several tens to hundreds of kilometers, which we call "mesoscale," mean vertical motion is very small compared to mean horizontal motion. Yet the vertical motion exerts a critical influence on the formation of clouds: Large-scale descent is associated with fair weather, and ascent is associated with cloudiness. Weather and climate modeling often assumes that mesoscale vertical motion varies slowly in the three spatial dimensions and with time. Recent observations over the tropical Atlantic, however, showed strong variability in mesoscale vertical motion, implying that clouds do not only respond to vertical motion but may themselves trigger vertical motion in their vicinity. This study reports similar variability also near Darwin, Australia. One way in which clouds can trigger remote vertical motion is by emitting waves, similar to stones that are thrown into a pond. This study examines vertical profiles of horizontal wind speed that were measured by instruments on ascending balloons near Darwin, Australia. These observations do indeed show waves that can provide a plausible explanation for the patterns of noteworthy variability in mesoscale motions. These findings suggest a two-way coupling of clouds to their environment with potentially important consequences for our understanding of weather and climate phenomena.

1. Introduction

Although gravity waves (GWs) are generated mainly in the troposphere, most research has been concerned with their effects on the middle and upper atmosphere, where they are key drivers of the large-scale circulation (e.g., Alexander et al., 2010; Holton, 1982, 1983). Yet it has been known for many decades that GWs also constitute an important component of tropospheric dynamics across a range of spatial and temporal scales. For instance, GWs can promote the growth of shallow convection into long-lived convective bands (Shige & Satomura, 2001), initiate severe convection (Balaji & Clark, 1988; Su & Zhai, 2017), induce quasi-regularly spaced cloud systems (Lane & Zhang, 2011), or provide a mechanism for the longevity of convective systems (Lane & Zhang, 2011; Stechmann & Majda, 2009). Diabatic heating from condensation is an efficient source of GWs, which may in turn suppress, favor, or trigger remote convection by inducing mesoscale rising or sinking motion, respectively (e.g., Mapes, 1993; Stephan et al., 2016). In this sense, clouds are sources as well as sinks of wave energy and able to remotely condition the surrounding environment for subsequent convection.

Here, we diagnose the characteristics of low-frequency GWs from radiosonde observations in the troposphere, taken during the Tropical Warm Pool-International Cloud Experiment (TWP-ICE) that took place

in Darwin, Australia (130°E, 12°S) from 17 January to 13 February 2006 (May et al., 2008). Numerous studies have examined stratospheric and mesospheric GWs in the Darwin region during TWP-ICE (e.g., Evan & Alexander, 2008; Hecht et al., 2009; Hankinson et al., 2014a, 2014b) and during other campaigns (e.g., Lane et al., 2003; Tsuda et al., 2004). In contrast, there has been limited attention placed on tropospheric GWs (exceptions include Tsuda et al., 2004; Vincent et al., 2004), which are arguably more challenging than the stratospheric waves due to large temporal and spatial variations in stability and shear. Our study is the first to extract the characteristics of tropospheric GWs over this region and also the first to diagnose tropospheric divergence profiles linked directly to GWs. This tropospheric GW analysis is only able to be achieved by taking full advantage of the intensive observations from the TWP-ICE campaign as well as an additional variational data set over the Darwin region.

Our study is motivated by more recent observations over the tropical Atlantic near Barbados (Bony & Stevens, 2019). They diagnosed vertical profiles of divergence from dropsonde measurements of horizontal wind velocities. The sondes were released along circular flight paths of 180-km diameter. The resulting vertical profiles of area-averaged divergence showed a noteworthy wave-like structure (i.e., divergence and convergence) with magnitudes of variability of around 2×10^{-5} s^{-1} in the free troposphere. This is 4 times the climatological divergence required to balance radiative cooling. Surprisingly, these features were not short-lived but persisted for more than 1 hr. Furthermore, Bony and Stevens (2019) analyzed high-resolution nested simulations that were nudged to the observed conditions. The simulations also produced autocorrelation scales of the divergence in space and time of the order of 200 km and 4 hr, respectively. Bony and Stevens (2019) suggested a number of hypotheses, including cold pools or cooling at the melting layer, to explain the observed wave-like vertical structure of the mesoscale divergence profiles and the simulated scaling laws. GWs are one of these hypotheses, but this was not tested in the Bony and Stevens (2019) study.

The key aim of this study is to use detailed GW observations to test this hypothesis. GWs that may explain the divergence patterns need to have periods consistent with the temporal autocorrelation scales of the divergence profiles, horizontal wavelengths consistent with their spatial autocorrelation scales, and vertical wavelengths consistent with the vertical variability of the divergence profiles. At the same time GWs obey a dispersion relation, which relates their period, horizontal, and vertical wavelengths. Thus, as these GW characteristics are not independent, GWs are not a trivial solution to the problem.

The TWP-ICE data set provides an excellent opportunity to investigate the influences of GWs on vertical profiles of mesoscale divergence. During the campaign 3-hourly radiosondes were launched from five stations, which were situated around an area of approximately 200-km diameter (Figure 1). Thus, the experimental domain is of similar size as the circular regions studied by Bony and Stevens (2019), and the soundings are of a sufficiently high temporal resolution to sample the relevant time scales. We will provide evidence that (i) vertical profiles of divergence near Darwin exhibit similar structures as those observed near Barbados, (ii) the previously reported autocorrelation timescales inferred from modeling can also be found in observations, and (iii) low-frequency GWs can serve as a potential explanation for the vertical, horizontal, and temporal structures of mesoscale divergence patterns.

Section 2 introduces the data from TWP-ICE that are analyzed for the properties of divergence and GWs in section 3. The results are discussed and summarized in section 4.

2. Data

The following is a brief summary of the synoptic and convective environment during the TWP-ICE campaign. More information can be found in May et al. (2008), where the TWP-ICE field experiment is described in detail. The campaign began with an active monsoon period that was characterized by rainfall rates of 17 mm/day averaged over the 300-km-diameter area sampled with a polarimetric radar at Darwin. The degree of convective organization differed widely and a major mesoscale convective system developed on 23 January. A suppressed monsoon period followed from 28 January to 6 February before deep convection featuring intense afternoon thunderstorms and some squall lines commenced again in the monsoon break period 7–13 February. The suppressed period was characterized by surface westerly winds and midlevel advection of dry continental air, which limited convection to isolated cells or short lines with only few deep single cells reaching up to 10 km. The average rain rates were 5–7 mm/day and originated from relatively shallow convection. The three days following 3 February were completely clear with no rain. We will focus on this 10-day suppressed period 28 January to 6 February, as it presents the most undisturbed conditions in the

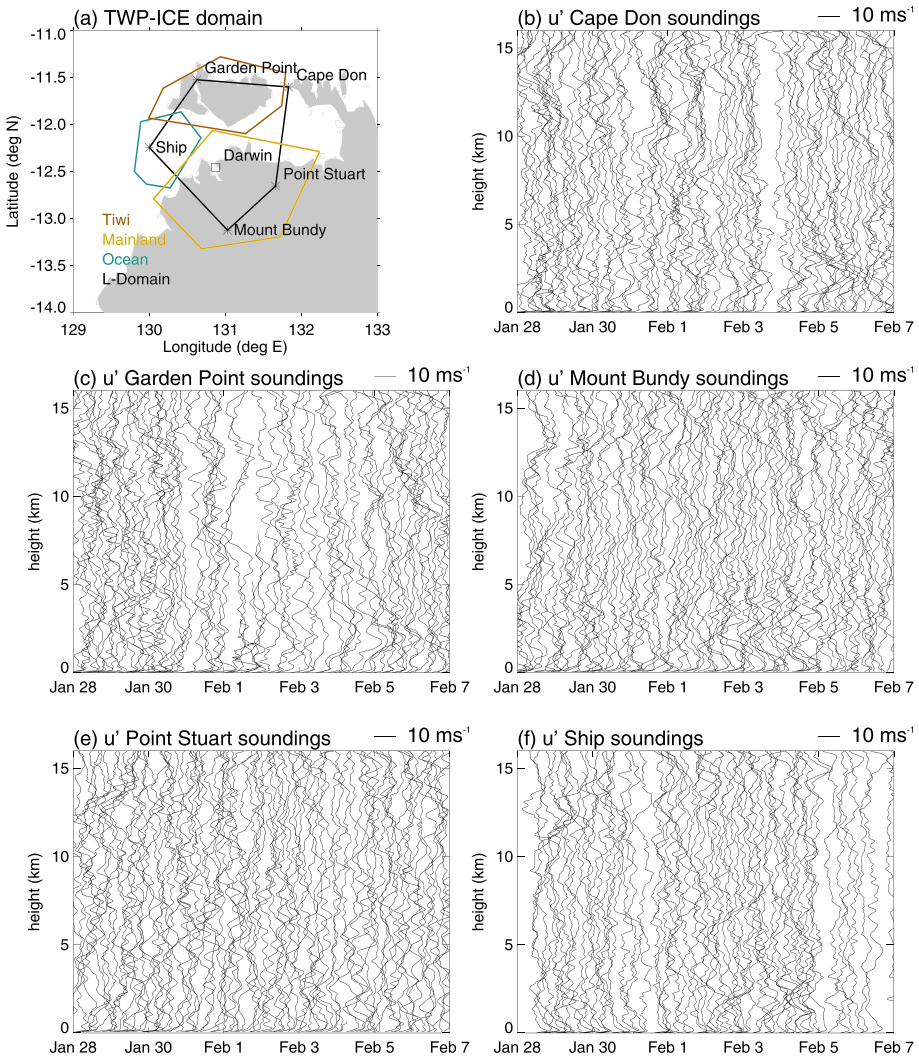

Figure 1. (a) Locations of Darwin and the five radiosonde launching sites during TWP-ICE. L-Domain (black) encloses the five boundary forcing stations. Subdomains are shown with colored lines. (b–f) For each launch location the zonal wind perturbations u' from radiosonde soundings interpolated to a 10-m vertical grid. u' are deviations from the area-mean horizontal wind speed of the variational analysis on L-Domain.

troposphere, allowing the extraction of wave signatures from tropospheric wind perturbations that at other times would be obfuscated by convection or turbulence. Moreover, the atmospheric conditions inside the TWP-ICE domain during the suppressed period are similar to the environment sampled by the circle flights analyzed in Bony and Stevens (2019), where intermittent shallow cumulus convection was observed.

Area-averaged divergence is taken from variational analysis data. By following the objective method of Zhang and Lin (1997), Xie et al. (2010) created a variational analysis for the TWP-ICE domain, which we will refer to as the large domain, or "L-Domain," as well as separate variational analyses for subdomains (Figure 1a). The variational analysis technique combines a background from the European Centre for Medium-Range Weather Forecasts (ECMWF) operational analysis with constraints from satellite, surface, and radiosonde measurements taken during TWP-ICE. It includes as boundary forcing the observations from radiosondes launched inside the respective domains. The technique applies small perturbations to the observed profiles of temperature, wind, and humidity, in order to conserve column-integrated mass, moisture, energy, and momentum, while limiting perturbation magnitudes to observational uncertainty. In this way the area-averaged time-evolving vertical profiles of thermodynamic variables are obtained. The variational analysis method was shown to be superior to other methods of computing area-averaged divergence, for instance, the line integral method, because it balances the heat and water budget at the same

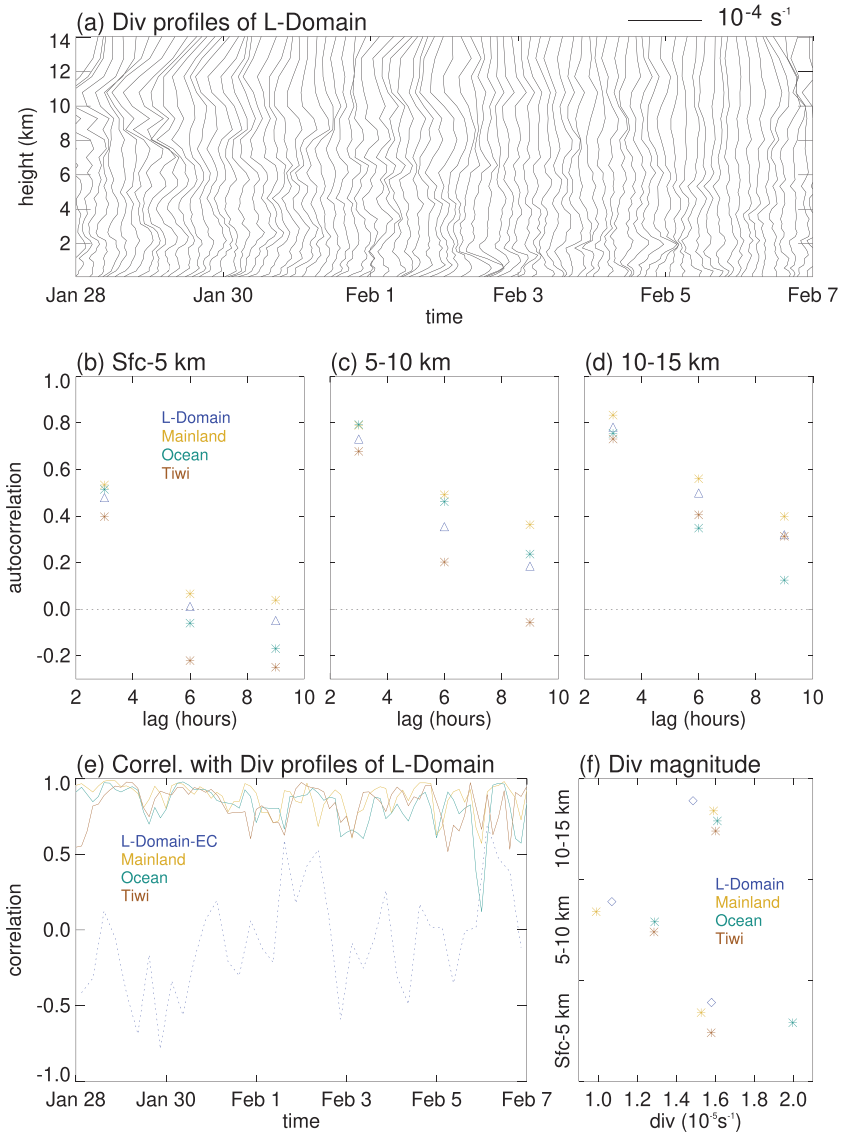

Figure 2. Characteristics of large-scale divergence from the variational analyses for the suppressed period 28 January 00:00 UTC to 7 February 00:00 UTC. (a) Three-hourly vertical profiles of divergence on L-Domain. (b–d) Autocorrelations of divergence vertically averaged over (a) surface—5 km, (b) 5–10 km, and (c) 10–15 km for all domains. (e) Correlations of the vertical divergence profiles between 2 and 14 km with that of L-Domain. L-Domain-EC (dashed) denotes the variational analysis on L-Domain that is based on virtual soundings from the ECMWF analysis. (f) Time-averaged divergence amplitude in the vertical layers, which are labeled on the *y* axis (defined as the time average of the maximum absolute value within each layer). Data points for the different variational analyses are vertically offset for better visibility.

time as providing the traditional line integral only based terms (Zhang & Lin, 1997; Zhang et al., 2001). In addition, Davies et al. (2013) repeated the variational analysis for L-Domain based on ECMWF data only ("L-Domain-EC"). Instead of ingesting radiosonde measurements, they replaced them with vertical profiles from ECMWF grid points near the respective radiosonde launch locations.

Measurements from 3-hourly radiosonde soundings at five stations (Ship, Cape Don, Garden Point, Mount Bundy, and Point Stuart; Figure 1) are analyzed for GW signatures. Winds, air temperature, mixing ratio, pressure, and the altitude of the balloons were recorded every 2 s. As in Hankinson et al. (2014a), we use area-averaged vertical profiles of U and V from the variational analysis on L-Domain to derive perturbations u' and v' from radiosonde measurements, which are then analyzed for GWs (Figure 1b-f). Furthermore, we intercompare divergence profiles from variational analyses on different domains to test

how their characteristics vary in space and with domain size and boundary forcing (i.e., L-Domain versus L-Domain-EC).

Several studies have shown that a rich spectrum of stratospheric GWs with sources near Indonesia existed during TWP-ICE (Evan & Alexander, 2008; Evan et al., 2012; Hecht et al., 2009; Hankinson et al., 2014a, 2014b). Our study is the first to investigate GWs during TWP-ICE with a specific focus on the troposphere.

3. Results

3.1. Vertical Profiles of Divergence

Figure 2a shows the temporal evolution of vertical profiles of divergence from the variational analysis on L-Domain, which uses the full TWP-ICE sounding array as the fundamental data set. Typical magnitudes of divergence are $\pm 2 \times 10^{-5}$ s^{-1}, as can also be seen from Figure 2f. The profiles show a rich spectrum of rather persistent or oscillating wave-like signals. At a 3-hr lag, temporal autocorrelations for L-Domain are ~0.5 for divergence averaged between the surface and 5 km (Figure 2b), ~0.7 for averages between 5 and 10 km (Figure 2c), and close to 0.8 for 10–15 km (Figure 2d). At a 9-hr lag time, they drop to zero below 5 km and to 0.2 at higher levels. More consistent signals in the upper troposphere are expected because the lower troposphere is noisier due to its proximity to the boundary layer and shallow convection.

It is insightful to intercompare the divergence profiles of the different subdomains, as they are spatially separated and ingest data from independent soundings. The vertical profiles of all subdomains are strongly correlated with that of L-Domain at all times (Figure 2e). In contrast, L-Domain-EC does not capture the vertical structure of divergence. This suggests that all soundings are subject to a similar large-scale forcing of divergence, which is not included in the ECMWF analysis. The ECMWF analysis used for L-Domain-EC assimilated only the 6-hourly soundings from Darwin and was available for ingestion into the variational analysis algorithm at a longitude-latitude resolution of 0.5° × 0.5° and 15 vertical levels between 1,000 and 10 hPa.

Unsurprisingly given Figure 2e, all subdomains have similar autocorrelation timescales (Figures 2b–2d). In addition, their magnitudes of temporal variability are similar, within $\pm 0.5 \cdot 10^{-5}$ s^{-1} (Figure 2f). This suggests that any mechanism responsible for the observed variability of divergence must be sufficiently large in scale to simultaneously affect all TWP-ICE domains used here.

3.2. GWs

We next investigate if GWs may explain the observed characteristics of the vertical profiles of large-scale divergence. The divergence $Div(x, y, z, t)$ is directly related to the wind perturbations associated with a plane wave with wave vector (k, l, m), frequency ω and phase ϕ:

$$(u, v, w) = (A_x, A_y, A_z) e^{i(kx+ly+mz-\omega t+\phi)}, \tag{1}$$

as

$$Div \sim (kA_x + lA_y) \sin(kx + ly + mz - \omega t + \phi). \tag{2}$$

To first order, the intrinsic frequencies of GWs are bound by the inertial frequency f, which at Darwin would correspond to a period of 57.6 hr, and the buoyancy frequency N, which would correspond to periods of less than 10 min in the midtroposphere during TWP-ICE. We focus on low-frequency waves with periods of 0.5–1.5 days, as the typical periods and horizontal wavelengths of high-frequency GWs are too short to simultaneously affect an area of the size of L-Domain. As described earlier, we obtain wave perturbations of the zonal and meridional velocities, u' and v', by subtracting the respective vertical profiles from the variational analysis on L-domain. The resulting profiles of u' are shown in Figures 1b–1f. The wind perturbations exhibit consistency between subsequent profiles; that is, they are associated with low-frequency, long-wavelength, waves. These wind perturbations are not mere noise but contain coherent physical features, as is revealed by vertical phase propagation between subsequent soundings. Yet while single stations are often dominated by one particular wave for the duration of several hours, there is no consistent signal of phase propagation between the different stations. This suggests that at any given time and location, multiple GWs are present. For this reason, we do not attempt to extract a single predominant wave at any time but choose a statistical approach to determine the average properties of the spectrum of inertia GWs passing the TWP-ICE domain.

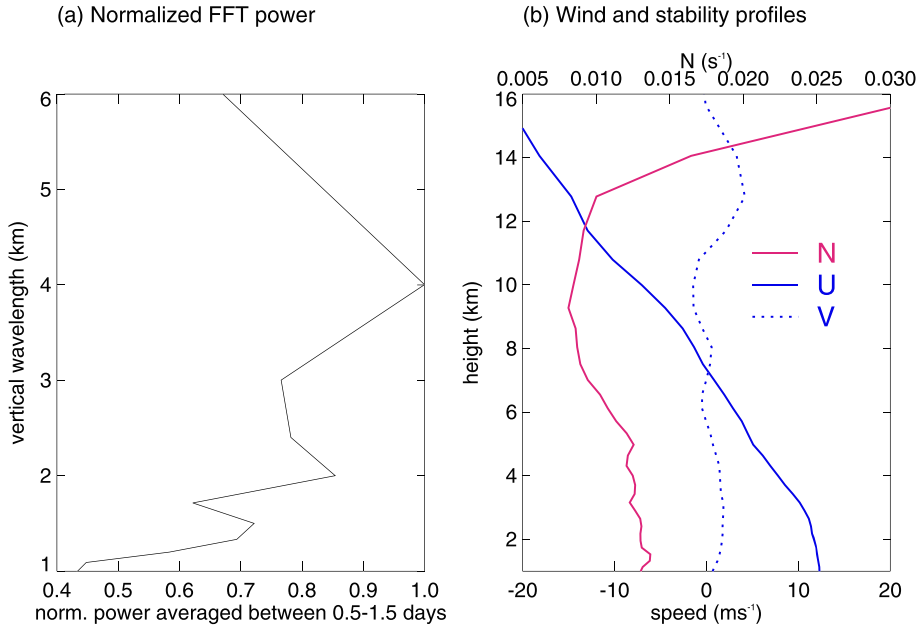

Figure 3. (a) The quadrature spectrum of u' and v' for the suppressed period 28 January 00:00 UTC to 7 February 00:00 UTC averaged over all five radiosonde stations and over periods of 0.5–1.5 days. The spectrum is normalized by its peak. u' and v' are the deviations from the variational analysis on L-Domain and were first interpolated to vertical and temporal resolutions of 10 m and 10,000 s, respectively. (b) Average background profiles of U, V, and N from the variational analysis on L-Domain for the suppressed period.

The main spectral peak of the low-frequency GW spectrum is identified by computing the quadrature spectrum of u' and v' as a function of the ground-based frequency ω_{gb} and the vertical wavenumber m. Since this requires evenly spaced data points in time and height, u' and v' are first interpolated to a 10-m resolution in the vertical and to a 10,000-s resolution in time, which roughly corresponds to the average radiosonde launch interval. The TWP-ICE soundings were not evenly spaced in time and the number of soundings differ between the stations. The spectral analysis is carried out between 2- and 14-km altitudes to avoid the boundary layer and the tropopause. Not all soundings reach 14 km and there are intervals of missing data, as can be seen from Figures 1b–1f. We treat missing observations by linearly interpolating in time from values observed at the same altitude.

Figure 3a shows the quadrature power spectrum of u' and v' averaged over all stations after integrating over periods of 0.5–1.5 days. We analyze the peak at $\lambda_z = 4$ km. To isolate perturbations in the relevant spectral region, u' and v' are first filtered in Fourier space. We retain ground-based periods $\tau_{gb} = 0.5$–1.5 days, $\lambda_z =$ 3.5–4.5 km. The filtered wind perturbations are subjected to the Stokes parameter method developed by Eckermann and Vincent (1989). The horizontal wind perturbation vector of low-frequency GWs rotates with height, such that the wave's hodograph follows a polarization ellipse. The Stokes algorithm diagnoses key parameters of these ellipses. The angle θ of the counterclockwise rotation of the major axis from the eastward direction corresponds to the propagation direction of the wave (with a 180° ambiguity). Here, the average θ is −12° for $\lambda_z = 4$ km (Table 1). Thus, the waves are propagating either nearly due eastward or westward. Studies investigating stratospheric waves showed eastward propagation (see section 2), and this is plausible as data from the Tropical Rainfall Measuring Mission (Huffman et al., 2014) show that convection is always present to the west and north over the Maritime Continent during the analyzed period (not shown). To confirm that the strong deep convective activity in this area remained similar during the period 28 January to 6 February, we obtain Tropical Rainfall Measuring Mission data for a 60° wide conical sector to the north-northwest of Darwin, that is, a wedge spanning 60° from due north. For source radii of 1,000 and 2,000 km we compute daily means of the area fraction where 3-hourly precipitation rates exceeded 10 mm. During the period 28 January to 6 February these fractions vary within one standard deviation between 0.5–2.6% (1,000-km radius) and 1.1–2.5% (2,000-km radius). Thus, it is plausible that the Maritime Continent is the source region of the waves observed over the Darwin region.

Table 1
Gravity Wave Properties for $\lambda_z = 4$ km Derived From Radiosonde Soundings

Station	θ (°)	τ_* (hr)	λ_h (km)	τ^*_{200} (hr)
Garden Point	20	20.9	770	5.4
Mount Bundy	21	2.3	750	5.4
Point Stuart	−37	12.4	440	5.7
Ship	−42	11.3	400	5.7
Cape Don	−24	15.5	550	5.6
Average	−12	12.5	580	5.6

Note. θ is the propagation direction measured counterclockwise from eastward, τ_* is the intrinsic period, λ_h the horizontal wavelength, and τ^*_{200} the time it takes a wave to travel 200 km when there is no background wind.

The ratio R of the major to minor axis of the polarization ellipse is used to estimate the typical intrinsic frequency of the inertia GWs as

$$\omega_* = \frac{f}{R}. \tag{3}$$

Background wind shear transverse to propagation direction of a wave can create an additional eccentricity (e.g., Cho, 1995; Hines, 1989). Here, we can neglect the corresponding correction term, as shear in the transverse direction; that is, the meridional direction is close to 0 (Figure 3b).

The horizontal wavenumber k is calculated from the GW dispersion relation as

$$k^2 = \frac{\left(\omega_*^2 - f^2\right)\left(m^2 + \frac{1}{4H_s^2}\right)}{N^2}, \tag{4}$$

where H_s is the density scale height and N the mean buoyancy frequency. To evaluate equation (4), we insert for m the wavenumber corresponding to $\lambda_z = 4$ km. Intrinsic periods and horizontal wavelengths vary substantially from station to station (Table 1). This may in part be due to noise and the effects of missing data. But a certain variability from station to station is also physically plausible, as we expect the tropospheric GW background to consist of a wide spectrum of waves and different waves may dominate at a given location. The average intrinsic period is 12.5 hr, and the horizontal wavelength is on average $\lambda_h = 580$ km. Thus, areas spanning roughly $\frac{1}{2}\lambda_h \sim 300$ km would experience similar conditions in terms of GW-driven divergence. This is consistent with the high correlations between the vertical divergence profiles from the variational analyses on different subdomains (Figure 2e). It is also consistent with a lack of sensitivity of the magnitude of temporal variability to the domain area, as all domains fit well within half a horizontal wavelength.

In calm wind conditions rising or sinking motion at any given location would prevail for the duration of half the intrinsic period, that is, 4 to 6 hr. This timescale is consistent with the temporal autocorrelations of divergence (Figures 2b–2d). Note that the mean wind over the domain is indeed close to 0 (Figure 3b). A wave crest would take approximately 5.6 hr to traverse a region of 200-km diameter. This timescale is rather insensitive to the station (Table 1), because it depends only on the phase speed $c_h = \frac{\omega_*}{k_h}$, which is similar for all stations (10 m/s). In addition to the period of a wave, the latter timescale may also be important for explaining the autocorrelation times of divergence, as it implies that a crest of one wave can dominate the divergence field averaged over areas of 200-km diameter for roughly 6 hr.

4. Conclusion

We demonstrated that vertical profiles of divergence near Darwin obtained during the TWP-ICE campaign exhibit similar wave-like structures as those observed over the tropical Atlantic. Bony and Stevens (2019) reported values of 2×10^{-5} s^{-1} for the magnitudes of divergence variability in layers of a few kilometers thickness. This magnitude of variability is in excellent agreement with TWP-ICE data (Figure 2f). The observations discussed by Bony and Stevens (2019) were taken over the ocean, while the TWP-ICE observations were mainly taken over land. Both studies examined convectively suppressed conditions during local summer at mirroring latitudes. The similar absolute value of the Coriolis parameter may partly explain the

similarities between the different locations, as it enters the GW dispersion relation and acts as a lower bound on the range of wave intrinsic frequencies. The autocorrelations reported by Bony and Stevens (2019) were based on high-resolution simulations, which were initialized and nudged at their boundary using data from the Integrated Forecast System of the ECMWF. They inferred temporal autocorrelation scales of 4 hr for circular regions of 100-km radius, which is confirmed by the observations from TWP-ICE. The autocorrelation timescale of divergence agrees very well with the characteristic GW timescales derived here. TWP-ICE data do not allow us to test spatial autcorrelation scales, which were 2.2° of latitude over the tropical Atlantic (Bony & Stevens, 2019). This distance corresponds to the typical GW horizontal wavelengths found for Darwin, such that GW dynamics would be able to explain the spatial correlations as well. Thus, low-frequency GWs can serve as a plausible explanation for the vertical, horizontal, and temporal structures of mesoscale divergence patterns.

The existence of strong convergence or divergence layers implies that the mesoscale environment is potentially strongly influenced by physical processes other than those usually included in climate models. Large parts of the GW spectrum are not captured in climate models of coarse resolution. The typical effective horizontal and vertical resolutions are hardly sufficient for resolving the waves, let alone their sources. The scales discussed here are large compared to single updrafts but correspond well to scales of organized convection. Thus, low-frequency GWs might be important for determining the characteristics of cloudiness on the mesoscale. Clouds and their coupling to circulation still remain one of the major uncertainties in climate predictions (Bony et al., 2015). The temporal and spatial scales reported here can serve as guidance for measurements during future field campaigns, such as the field campaign Elucidating the Role of Cloud-Circulation Coupling in Climate (EUREC4A Bony et al., 2017), which will take place in winter 2020, and could be used to collect additional data for analyzing the response of convection to GW dynamics in relation to other cloud controlling factors. The relatively short inertial periods of the waves (Table 1) favor soundings at short intervals, ideally every 2 hr. Given that the hodograph method can be independently applied to data at single locations, one station with high-frequency soundings would already be an improvement over, for example, an array of locations with 6-hourly soundings. Moreover, if soundings at different locations within several hundreds of kilometers were launched exactly simultaneously, this may allow a direct computation of the horizontal wavelengths by inferring the phase differences between different locations.

Inertia GWs are able to propagate large distances inside the troposphere. Based on their large spatial scales and the fact that convective sources always exist at some location in the tropics, we expect such waves to be present most of the time. What remains unclear is to what degree the tropospheric wave background is saturated or consists of individual spectral peaks or individual waves. This would also help us to understand what fraction of variability in our results is physical. We have shown here that GWs are a plausible explanation for patterns of mesoscale divergence at two different locations. To prove that they really are the cause for these patterns, additional measurements as well as numerical experiments are needed. A better knowledge of the statistical properties of the wave background and its relationship to convection is desirable and should be the goal of future investigations.

Acknowledgments

C. C. Stephan was supported by the Minerva Fast Track Programme of the Max Planck Society. T. P. Lane and C. Jakob were supported by the ARC Centre of Excellence for Climate Extremes (CE170100023). C. C. Stephan is grateful for the joint funding from the ARC Centre of Excellence for Climate Extremes (CE170100023) and the Max Planck Institute for Meteorology to enable the research visit to Australia that has led to the research reported here. The authors also acknowledge the support of the U.S. Department of Energy Atmospheric Radiation Measurement (ARM) Program for the TWP-ICE campaign. The data used in this study are available from the ARM data archive (https://www.arm.gov/data).

References

Alexander, M. J., Geller, M., McLandress, C., Polavarapu, S., Preusse, P., Sassi, F., & Watanabe, S. (2010). Recent developments in gravity-wave effects in climate models and the global distribution of gravity-wave momentum flux from observations and models. *Quarterly Journal of the Royal Meteorological Society*, *136*(650), 1103–1124. https://doi.org/10.1002/qj.637

Balaji, V., & Clark, T. L. (1988). Scale selection in locally forced convective fields and the initiation of deep cumulus. *Journal of the Atmospheric Sciences*, *45*, 3189–3211. https://doi.org/10.1175/1520-0469(1988)045<3188

Bony, S., & Stevens, B. (2019). Measuring area-averaged vertical motions with dropsondes. *Journal of the Atmospheric Sciences*, *76*, 767–783. https://doi.org/10.1175/JAS-D-18-0141.1

Bony, S., Stevens, B., Ament, F., Bigorre, S., Chazette, P., Crewell, S., & Wirth, M. (2017). EUREC4A: A field campaign to elucidate the couplings between clouds, convection and circulation. *Surveys in Geophysics*, *38*(6), 1529–1568. https://doi.org/10.1007/s10712-017-9428-0

Bony, S., Stevens, B., Frierson, D. M. W., Jakob, C., Kageyama, M., Pincus, R., & Webb, M. J. (2015). Clouds, circulation and climate sensitivity. *Nature Geoscience*, *8*, 261. https://doi.org/10.1038/ngeo2398

Cho, J. Y. N. (1995). Inertio-gravity wave parameter estimation from cross-spectral analysis. *Journal of Geophysical Research*, *100*(D9), 18727–18737. https://doi.org/10.1029/95JD01752

Davies, L., Jakob, C., May, P., Kumar, V. V., & Xie, S. (2013). Relationships between the large-scale atmosphere and the small-scale convective state for Darwin, Australia. *Journal of Geophysical Research: Atmospheres*, *118*, 11,534–11,545. https://doi.org/10.1002/jgrd.50645

Eckermann, S. D., & Vincent, R. A. (1989). Falling sphere observations of anisotropic gravity wave motions in the upper stratosphere over Australia. *Pure and Applied Geophysics*, *130*, 509–532. https://doi.org/10.1007/BF00874472

Evan, S., & Alexander, M. J. (2008). Intermediate-scale tropical inertia gravity waves observed during the TWP-ICE campaign. *Journal of Geophysical Research*, *113*, D14104. https://doi.org/10.1029/2007JD009289

Evan, S., Alexander, M. J., & Dudhia, J. (2012). Model study of intermediate-scale tropical inertia-gravity waves in comparison to TWP-ICE campaign observations. *Journal of the Atmospheric Sciences*, *69*, 591–610. https://doi.org/10.1175/JAS-D-11-051.1

Hankinson, M. C. N., Reeder, M. J., & Lane, T. P. (2014a). Gravity waves generated by convection during TWP-ICE: I. Inertia-gravity waves. *Journal of Geophysical Research: Atmospheres*, *119*, 5269–5282. https://doi.org/10.1002/2013JD020724

Hankinson, M. C. N., Reeder, M. J., & Lane, T. P. (2014b). Gravity waves generated by convection during TWP-ICE: 2. High-frequency gravity waves. *Journal of Geophysical Research: Atmospheres*, *119*, 5257–5268. https://doi.org/10.1002/2013JD020726

Hecht, J. H., Alexander, M. J., Walterscheid, R. L., Gelinas, L. J., Vincent, R. A., MacKinnon, A. D., & Russell III, J. M. (2009). Imaging of atmospheric gravity waves in the stratosphere and upper mesosphere using satellite and ground-based observations over Australia during the TWPICE campaign. *Journal of Geophysical Research*, *114*, D18123. https://doi.org/10.1029/2008JD011259

Hines, C. O. (1989). Tropopausal mountain waves over Arecibo: A case study. *Journal of the Atmospheric Sciences*, *46*, 476–488. https://doi.org/10.1175/1520-0469(1989)046<0476

Holton, J. R. (1982). The role of gravity wave induced drag and diffusion in the momentum budget of the mesosphere. *Journal of the Atmospheric Sciences*, *39*, 791–799. https://doi.org/10.1175/1520-0469(1982)039<0791:TROGWI>2.0.CO;2

Holton, J. (1983). The influence of gravity wave breaking on the general circulation of the middle atmosphere. *Journal of the Atmospheric Sciences*, *40*, 2497–2507. https://doi.org/10.1175/1520-0469(1983)040<2497:TIOGWB>2.0.CO;2

Huffman, G., Bolvin, D., Braithwaite, D., Hsu, K., Joyce, R., & Xie, P. (2014). Integrated Multi-satellitE Retrievals for GPM (IMERG), version 4.4. NASA's Precipitation Processing Center.

Lane, T. P., Reeder, M. J., & Guest, F. M. (2003). Convectively generated gravity waves observed from radiosonde data taken during MCTEX. *Quarterly Journal of the Royal Meteorological Society*, *129*, 1731–1740. https://doi.org/10.1256/qj.02.196

Lane, T. P., & Zhang, F. (2011). Coupling between gravity waves and tropical convection at mesoscales. *Journal of the Atmospheric Sciences*, *68*, 2582–2598. https://doi.org/10.1175/2011JAS3577.1

Mapes, B. E. (1993). Gregarious tropical convection. *Journal of the Atmospheric Sciences*, *50*, 2026–2037. https://doi.org/10.1175/1520-0469(1993)050<2026:GTC>2.0.CO;2

May, P. T., Mather, J. H., Vaughan, G., Jakob, C., McFarquhar, G. M., Bower, K. N., & Mace, G. G. (2008). The Tropical Warm Pool-International Cloud Experiment. *Bulletin of the American Meteorological Society*, *89*, 629–645. https://doi.org/10.1175/BAMS-89-5-629

Shige, S., & Satomura, T. (2001). Westward generation of eastward-moving tropical convective bands in TOGA COARE. *Journal of the Atmospheric Sciences*, *58*, 3724–3740. https://doi.org/10.1175/1520-0469(2001)058<3724

Stechmann, S. N., & Majda, A. J. (2009). Gravity waves in shear and implications for organized convection. *Journal of the Atmospheric Sciences*, *66*, 2579–2599. https://doi.org/10.1175/2009JAS2976.1

Stephan, C. C., Alexander, M. J., & Richter, J. H. (2016). Characteristics of gravity waves from convection and implications for their parameterization in global circulation models. *Journal of the Atmospheric Sciences*, *73*, 2729–2742. https://doi.org/10.1175/JAS-D-15-0303.1

Su, T., & Zhai, G. (2017). The role of convectively generated gravity waves on convective initiation: A case study. *Monthly Weather Review*, *145*, 335–359. https://doi.org/10.1175/MWR-D-16-0196.1

Tsuda, T., Ratnam, M. V., May, P. T., Alexander, M. J., Vincent, R. A., & MacKinnon, A. (2004). Characteristics of gravity waves with short vertical wavelengths observed with radiosonde and GPS occultation during DAWEX (Darwin Area Wave Experiment). *Journal of Geophysical Research*, *109*, D20S03. https://doi.org/10.1029/2004JD004946

Vincent, R. A., MacKinnon, A., Reid, I. M., & Alexander, M. J. (2004). VHF profiler observations of winds and waves in the troposphere during the Darwin Area Wave Experiment (DAWEX). *Journal of Geophysical Research*, *109*, D20S02. https://doi.org/10.1029/2004JD004714

Xie, S., Hume, T., Jakob, C., Klein, S. A., McCoy, R. B., & Zhang, M. (2010). Observed large-scale structures and diabatic heating and drying profiles during TWP-ICE. *Journal of Climate*, *23*, 57–79. https://doi.org/10.1175/2009JCLI3071.1

Zhang, M. H., & Lin, J. L. (1997). Constrained variational analysis of sounding data based on column-integrated budgets of mass, heat, moisture, and momentum: Approach and application to ARM measurements. *Journal of the Atmospheric Sciences*, *54*, 1503–1524. https://doi.org/10.1175/1520-0469(1997)054<1503

Zhang, M. H., Lin, J. L., Cederwall, R. T., Yio, J. J., & Xie, S. C. (2001). Objective analysis of ARM IOP data: Method and sensitivity. *Monthly Weather Review*, *129*(2), 295–311. https://doi.org/10.1175/1520-0493(2001)129<0295:OAOAID>2.0.CO;2